



Lawrence Berkeley Laboratory

UNIVERSITY OF CALIFORNIA

RECEIVED
LIBRARY
BERKELEY CALIFORNIA

FEB 9 1987

DOCUMENTS SECTION

Submitted to Physical Review C

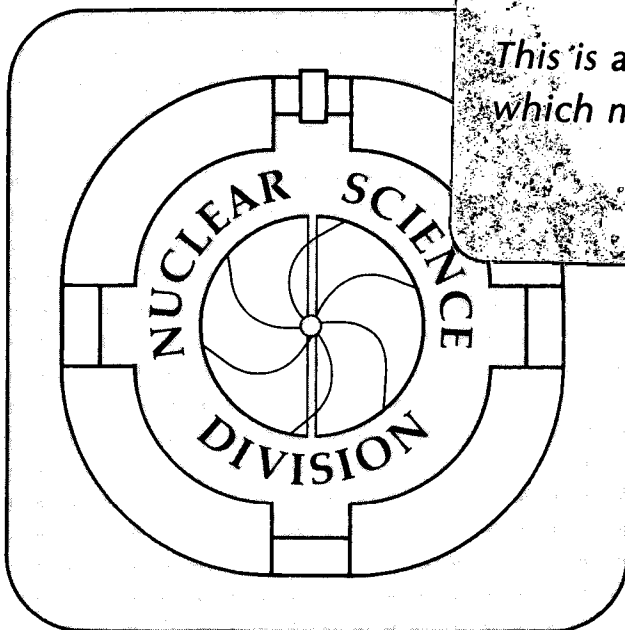
PROBING THE DIRECT STEP OF RELATIVISTIC
HEAVY ION FRAGMENTATION — ($^{12}\text{C}, ^{11}\text{B}+p$)
AT 2.1 GeV/NUCLEON WITH C AND CH_2 TARGETS

M.L. Webb, H.J. Crawford, J. Engelage,
M.E. Baumgartner, D.E. Greiner, P.J. Lindstrom,
D.L. Olson, and R. Wada

December 1986

TWO-WEEK LOAN COPY

*This is a Library Circulating Copy
which may be borrowed for two weeks*



LBL-22556
22

DISCLAIMER

This document was prepared as an account of work sponsored by the United States Government. While this document is believed to contain correct information, neither the United States Government nor any agency thereof, nor the Regents of the University of California, nor any of their employees, makes any warranty, express or implied, or assumes any legal responsibility for the accuracy, completeness, or usefulness of any information, apparatus, product, or process disclosed, or represents that its use would not infringe privately owned rights. Reference herein to any specific commercial product, process, or service by its trade name, trademark, manufacturer, or otherwise, does not necessarily constitute or imply its endorsement, recommendation, or favoring by the United States Government or any agency thereof, or the Regents of the University of California. The views and opinions of authors expressed herein do not necessarily state or reflect those of the United States Government or any agency thereof or the Regents of the University of California.

Probing the Direct Step of Relativistic Heavy
Ion Fragmentation — ($^{12}\text{C}, ^{11}\text{B}+\text{p}$) at 2.1
GeV/Nucleon with C and CH_2 targets*.

M. L. Webb

University of California at Davis
Davis, California 95616

H. J. Crawford, J. Engelage

U. C. Space Science Laboratory
University of California at Berkeley
Berkeley, California 94720

M. E. Baumgartner[†], D. E. Greiner,
P. J. Lindstrom, D. L. Olson[‡], R. Wada[§]

Nuclear Science Division
Lawrence Berkeley Laboratory
University of California
Berkeley, California 94720

*This work was supported in part by the Director, Office of Energy Research, Division of Nuclear Physics of the Office of High Energy and Nuclear Physics of the U. S. Department of Energy under Contracts DE-AC03-76SF00098 and DE-AS05-76ER04699, in part by NSF grant PHY81-21003, and in part by NASA grant NGR-05-003-513.

[†]Current address Hoffman-LaRoche, Basel, Switzerland

[‡]Current address University of California at Riverside

[§]Current address Texas A and M University

Contents

1	Introduction	2
2	Experimental Setup	3
3	Results	4
3.1	Introduction	4
3.2	Monte Carlo Cascade Model	6
3.3	^{11}B Inclusive Spectra	8
3.4	Proton Exclusive Spectra	9
3.5	Residual Peak and Inelastic Cross Section	11
4	Conclusion	14
5	Acknowledgments	16
	References	17
	Table Captions	19
	Figure Captions	20

Probing the Direct Step of Relativistic Heavy Ion Fragmentation — ($^{12}\text{C}, ^{11}\text{B}+p$) at 2.1 GeV/Nucleon with C and CH_2 targets.

M. L. Webb

University of California at Davis

H. J. Crawford, J. Engelage

U. C. Space Science Laboratory

M. E. Baumgartner*, D. E. Greiner,

P. J. Lindstrom, D. L. Olson†, R. Wada‡

Lawrence Berkeley Laboratory

December 1986

Abstract

We have measured the momentum distributions and the excitation energy of the $p, ^{11}\text{B}$ pair in the ($^{12}\text{C}, ^{11}\text{B}+p$) reaction at 2.1 GeV/nucleon with C and CH_2 targets. The cross section separates into three regions, (1) nucleon-nucleon quasi-elastic scattering, (2) nucleon-nucleon inelastic scattering, and (3) a low excitation energy and momentum transfer peak. The cross sections, by region, are (1) 8.8 ± 2.5 mb, (2) 10.1 ± 2.2 mb, and (3) 0.81 ± 0.45 mb for $\text{H}(^{12}\text{C}, ^{11}\text{B}+p)\text{X}$ and (1) 11.1 ± 2.4 mb, (2) 24.1 ± 3.7 mb, and (3) 4.50 ± 0.67 mb for $\text{C}(^{12}\text{C}, ^{11}\text{B}+p)\text{X}$. The shapes of the first two regions can be fit with a nucleon-nucleon cascade model including π production. However, the cascade

*Current address Hoffman-LaRoche, Basel, Switzerland

†Current address University of California at Riverside

‡Current address Texas A and M University

model prediction for the quasi-elastic component is too large by a factor of three. The low momentum transfer peak is consistent with two mechanisms, (1) an excitation and decay via proton emission of the carbon projectile and (2) a projectile proton scattering diffractively off the C target. Finally, the Fermi momentum determined from the transverse momentum distribution is 160 ± 11 MeV/c compared to 190 ± 11 MeV/c from the longitudinal momentum distribution.

1 Introduction

Most theoretical models of relativistic heavy ion collisions use some variation of the participant-spectator[1] prescription. When the colliding nuclei interpenetrate, some nucleons in the overlap region scatter; these are the participants. The remaining nucleons comprise the projectile and target spectators. The process injects energy into the spectators and they can then decay by particle emission. Thus there are two types of sources each producing fragments by different mechanisms. In peripheral collisions the momentum signatures of the sources overlap and inclusive measurements[2,3,4] cannot adequately distinguish between them, allowing markedly different models[5,6,7] to explain the same results.

We will focus on the direct process in this paper. A simple reaction for studying the direct component of heavy ion fragmentation is ^{12}C fragmenting into $^{11}\text{B} + \text{p}$. There are two possibilities: (1) the proton is a participant and the ^{11}B is a spectator, or (2) the projectile is collectively excited and dissociates into a $^{11}\text{B}, \text{p}$ pair.

This dissociation process has been observed in $(^{12}\text{C}, 3\alpha)$ [8]. The simplicity of the $(^{12}\text{C}, ^{11}\text{B}+p)$ reaction offers the hope of an unambiguous comparison with the models and must be understood before more complicated reactions can be attempted with confidence.

To study this reaction one needs a measurement exclusive in projectile fragments. Previous quasi-exclusive measurements of this type have been made with photographic emulsions[9] and streamer chambers[10]. These approaches suffer from poor statistics. They also lack complete particle identification and cannot unambiguously select the reaction of interest.

The data presented here were measured at the Heavy Ion Superconducting Spectrometer (HISS) facility[11] at Lawrence Berkeley Laboratory. The aperture was large enough so that we were able to determine simultaneously the vector momenta of all charged projectile fragments down to zero momentum transfer over a region of phase space containing all the ^{11}B fragments and $72 \pm 19\%$ of the protons in the $\text{H}(^{12}\text{C}, ^{11}\text{B}+p)\text{X}$ reaction.

2 Experimental Setup

The experimental setup (Figure 1) included event trigger scintillators, a large volume magnetic dipole, 0.815 g/cm^2 C and 1.03 g/cm^2 CH_2 targets, track defining drift chambers and a scintillator wall for time of flight and charge determination. The trigger required a single ^{12}C to enter the dipole and no charge six particle in the

beam envelope after the dipole. The aperture (Figure 2) was limited by the second downstream drift chamber and the region of phase space covered by the momentum reconstruction code.

In the projectile frame, the proton momenta were measured to standard deviations of 10 MeV/c parallel to the beam and 7.7 MeV/c transverse. The corresponding ^{11}B standard deviations were 105 MeV/c and 32 MeV/c. The scintillator wall had a charge resolution of 0.1 charge units. Its time of flight resolution was 250 ps for the protons and 120 ps for the ^{11}B 's over a 7.6 m flight path. These gave mass resolutions of $80 \text{ MeV}/c^2$ for protons and $170 \text{ MeV}/c^2$ for ^{11}B 's. Requiring all proton tracks to point back to the target eliminated target out corrections to the 0.4% level. The proton detection efficiency was $80 \pm 5\%$ relative to that of the ^{11}B 's. This was due mainly to drift chamber inefficiencies.

3 Results

3.1 Introduction

We have measured two processes, $(^{12}\text{C}, ^{11}\text{B}+x)$ and $(^{12}\text{C}, ^{11}\text{B}+p)$. Only the first was entirely within the experimental aperture so $(^{12}\text{C}, ^{11}\text{B}+x)$ experimental cross sections were normalized to the ^{11}B inclusive measurements[3] of $30.9 \pm 3.4 \text{ mb}$ for the H target and $53.8 \pm 2.7 \text{ mb}$ for the C target. This allowed us to extract cross sections for the $(^{12}\text{C}, ^{11}\text{B}+p)$ process.

The projectile excitation energy spectra for ($^{12}\text{C}, ^{11}\text{B}+p$) in Figure 3 show two components, a low excitation energy peak and a long tail. Experimental energy resolution for this reaction, 6 MeV, precludes the identification of individual resonance peaks. Since we expect nucleon-nucleon scattering to be a major component of this cross section we next examine the proton spectra. These (Figure 4) display three features. (1) A ridge appears in the data along the line of nucleon-nucleon quasi-elastic scattering. The width of the ridge is a measure of the initial Fermi motion of the scattered nucleons. (2) There is also a plateau at lower rapidity. The large rapidity loss indicates that these are inelastic events. (3) A sharp peak appears at 100 MeV/c transverse momentum and beam rapidity. This is due to a low energy and momentum transfer process and is much stronger for the C target.

The ^{11}B spectra (Figure 5) display only a single peak, suggesting that the ^{11}B is indeed a minimally interacting participant to the reaction. The presence or absence of a simultaneously detected proton made no difference to the shape of the ^{11}B spectra, therefore we show only ^{11}B inclusive spectra.

It is useful to compare these proton and ^{11}B cross sections with free nucleon-nucleon scattering. For comparison to our data we used a Monte Carlo cascade model[7] with π production mediated through the Δ resonance, the dominant inelastic mechanism. This model is a sum of free nucleon-nucleon processes and any differences between it and the data can be attributed to collective effects.

In what follows we will first discuss the cascade model and the modifications

made. We then will compare the model and data for the ^{11}B inclusive spectra. Next a comparison for the proton exclusive spectra will be made. Finally we will discuss that part of the exclusive spectra which can not be fit by the cascade model.

3.2 Monte Carlo Cascade Model

The model has been changed[12] since its published description. The model has no binding energy, so the nuclei expanded with time. Freezing the nuclear distribution until an interaction occurs stops this. To better reflect knowledge about Δ production gained from proton-proton scattering[13], two changes were made. The Δ was given an exponential lifetime and the functional form of the Δ production cross section was changed. Of these changes only the latter significantly altered the model results for our case.

Under the original assumption of isotropic Δ production, only 20% of the protons from the decay of Δ 's were within the detector aperture. Using a production cross section of $\sigma(t) \propto e^{bt}$ where t is the Mandelstam t and $b = 10.11 \times 10^{-6} \text{ GeV}^{-2}$ [13], 53% of the protons from the decay of Δ 's are within the aperture. If the isotropic production cross section is used the cascade model cannot be reconciled with the the ratio of $(^{12}\text{C}, ^{11}\text{B}+p)$ to $(^{12}\text{C}, ^{11}\text{B}+x)$ measured. Finally, to better fit our data we use Fermi momentum as an adjustable parameter.

The major problem in comparing these cascade model results with the data is that the cascade model does not explicitly account for isospin. A significant fraction

of the Δ production channels involve charge exchange. If such a reaction leaves a neutron in the projectile frame it is indistinguishable from a $^{11}\text{B}+p$ event with the proton outside our aperture. Thus, for a valid comparison, the model predictions for the ^{11}B inclusive cross sections and the $(^{12}\text{C}, ^{11}\text{B}+p)$ cross sections in aperture must be consistent with the data. Fortunately charge independence holds well in this energy region[13] and this reaction channel is dominated by single nucleon-nucleon interactions, so it is possible to separate the cascade model results into components which can be weighted by isospin branching ratios.

To derive cross sections from the cascade model results we found the fraction of the interactions that scattered only one projectile nucleon. Any number of target nucleons were allowed to scatter. We then multiplied that fraction by the total fragmentation cross section to obtain a single nucleon scattering cross section. Using the total fragmentation cross section of 250 ± 10 mb for a H target[14] the cascade model predicts 100.4 ± 4.1 mb for single nucleon scattering with a H target. What follows is an analysis for a H target; the C target analysis is similar and both results are shown in Table I. Assuming the scattered projectile nucleon is a proton 50% of the time the cascade cross section for producing ^{11}B 's is 50.2 ± 2.0 mb, significantly higher than the previously measured value of 30.9 ± 3.4 mb[3]. We conclude that even at this basic level nucleus-nucleus collisions cannot be considered as just a sum of free nucleon collisions.

This cross section can be further separated into: (1) quasi-elastic scattering,

25.6 ± 1.1 mb, (2) Δ production in the projectile, 12.30 ± 0.52 mb, and (3) Δ production in the target, 12.30 ± 0.52 mb. From isospin considerations, 1/4 of the proton-proton collisions resulting in Δ 's in the target leave a proton in the projectile while 11/12 of the projectile Δ 's decay into a proton. The $^{11}\text{B}+x$ and $^{11}\text{B}+p$ cascade model cross sections for both targets are shown in Table I.

3.3 ^{11}B Inclusive Spectra

In the Monte Carlo cascade model the ^{11}B has a projectile frame momentum equal and opposite to the initial Fermi momentum of the scattered proton, so its spectrum (Figure 6) has the same shape for both targets. These spectra are inclusive since what happens to the proton after scattering is immaterial to the ^{11}B momentum distribution. To obtain the best fit to the data we allowed both the Fermi momentum and the cross section to vary in a χ^2 fit to the transverse momentum distribution.

The integral cross sections obtained from the fit were 18.6 ± 1.3 mb for the H target and 26.0 ± 1.7 mb for the C target. These are $60.2 \pm 2.9\%$ and $48.3 \pm 1.9\%$ of the data respectively. The difference is due to a tail at high transverse momentum which we excluded from the fit. The tail is more pronounced in the C target data and is absent from the model.

The Fermi momenta obtained from the fit were 160 ± 11 MeV/c for the H target and 160 ± 17 MeV/c for the C target. This differs from previous measurements of

221 MeV/c, derived from electron scattering [15] and 182 ± 5 MeV/c derived from fragment momentum distributions[4]. The difference between the latter value and our measurements is surprising since both use momentum distributions to derive the Fermi momentum. However our measurement is derived from the transverse momentum distribution while the other is derived from the longitudinal momentum distribution. Detector resolution made it meaningless to use our ^{11}B longitudinal momentum for comparison. However it is possible to extract the Fermi momentum from the proton longitudinal momentum (Section 3.4) and get a result that is consistent with the 182 ± 5 MeV/c measurement. This difference between the Fermi momenta determined from longitudinal and transverse momenta is inconsistent with the usual model of the nucleus as a free Fermi gas. It has been suggested[16] that this difference is due to the peripheral nature of the reaction, but no quantitative predictions have been made.

3.4 Proton Exclusive Spectra

The cascade model proton spectra (Figure 7) display two of the features that are in the proton data, the ridge and plateau. The ridge is due to nucleon-nucleon quasi-elastic scattering. The width of the ridge is dependent on the initial Fermi momentum. This is a longitudinal momentum measurement and should be equal to the previously measured 182 MeV/c[4]. The Fermi momenta fits were 190 ± 11 MeV/c for the H target and 190 ± 25 MeV/c for the C target. The low rapidity plateau is populated by inelastic scattering associated with π production. The

peaks at 100 MeV/c transverse momentum do not appear and the plateau shape is not duplicated well. These will be discussed later (Section 3.5). These spectra have been fit to the data and we discuss the fit and its implications next.

Having corrected the cascade model for charge exchange effects (Section 3.2) we can now compare the model prediction for ($^{12}\text{C}, ^{11}\text{B}+p$) in the detector aperture with the exclusive data. As with the ^{11}B inclusive data, scaling was required to get a good χ^2 fit. We found it necessary to vary both the quasi-elastic and inelastic cross sections as well as the Fermi momentum in fitting the cascade model proton spectra to the data. It was necessary to multiply the quasi-elastic components by $0.34 \pm 0.10\%$ for the H target and by $0.34 \pm 0.07\%$ for the C target. The inelastic components were scaled by $0.70 \pm 0.16\%$ for the H target and by $0.95 \pm 0.15\%$ for the C target. Thus the quasi-elastic component is smaller by a factor of three than what would be expected from free nucleon-nucleon scattering while the inelastic component is consistent with the prediction. This suppression of the quasi-elastic component shows clearly that the cascade model is not a valid microscopic description of the interaction process.

The fits were to the $-t$ distribution excluding the low momentum transfer peak (Figure 8). Here t is a modified Mandelstam $t = (\mathbf{p}_1 - \mathbf{p}_3)^2$, where $\mathbf{p}_1 = \mathbf{p}_{beam}/12$ before the reaction and $\mathbf{p}_3 = \mathbf{p}_{proton}$ after the reaction. The reduced mass of a nucleon within a ^{12}C nucleus is accounted for by using $\mathbf{p}_{beam}/12$. All \mathbf{p} are four-vectors. The modified Mandelstam t allows comparison to (p,p) scattering data. A

general check of the fit can be made by comparing the cascade model cross sections for ($^{12}\text{C}, ^{11}\text{B}+p$) in the aperture with the measured total cross section excluding the cross section in the peak (Section 3.5). This is done in Table II.

Having fit the ($^{12}\text{C}, ^{11}\text{B}+p$) spectra in the aperture we can estimate the aperture corrected ($^{12}\text{C}, ^{11}\text{B}+p$) cross sections by using the scaled cascade model values and the measured peak cross section. We can also determine the cascade model ($^{12}\text{C}, ^{11}\text{B}+x$) cross section. This latter cross section must be consistent with the ^{11}B inclusive data which was not used in the fit. The scaled cascade model plus peak underpredicts by $14 \pm 18\%$ for the H target and overpredicts by $12 \pm 15\%$ for the C target. These results are summarized in Table III.

3.5 Residual Peak and Inelastic Cross Section

Having normalized the cascade model we now focus on the unexplained regions of the data by subtracting the cascade model. The subtracted spectra (Figure 9) show two features: residual inelastic cross section in the low rapidity region and the low momentum transfer peaks. The large rapidity loss of the residual inelastic cross section indicates that other more highly inelastic processes must contribute to the inelastic region, such as $pp \rightarrow pp\pi^+\pi^-$. This is 6% of the free proton-proton total cross section[13].

The low momentum transfer peaks that remain are 0.81 ± 0.45 mb for the H target and 4.50 ± 0.67 mb for the C target. These cross sections were determined

by subtracting the normalized cascade model t spectra from the data t spectra (Figure 8). Here t is the previously defined modified Mandelstam t (Section 3.4).

Such peaks do appear in p-nucleus scattering. The $C(p,p)X$ cross section (Figure 10)[17] is shown as a function of the Mandelstam t . This plot can be fit by the sum of two exponentials, e^{86t} and $e^{5.2t}$. These can be interpreted as diffraction[18] from objects of radii 3.66 fm and 0.90 fm respectively, i.e. the C target nucleus and a target nucleon. Alternatively in the Glauber model[19] the low t peak is explained as the proton diffracting elastically off the target, while the rest of the cross section is due to excitations of the target. To allow such a process to occur in our case we follow the argument of Good and Walker[20]. Since the time of the interaction is short, the ^{12}C ground state and the low excitation energy $^{11}\text{B}+p$ states are essentially degenerate in energy. Thus it is possible for the proton to diffract elastically off the target while the ^{11}B is not affected. The cross section for this diffractive process has been calculated to be 10 % [21] of the $^{12}\text{C}(^{16}\text{O},^{15}\text{O}+x)X$ reaction at 2 GeV/nucleon.

To compare the p-nucleus data to our data, we show the proton cross section from the C target (Figure 11a) as a function of the previously defined modified Mandelstam t . Both diffractive peaks can be fit by e^{86t} . However our peak is 29 % or 4.50 ± 0.67 mb of the 15.6 ± 2.5 mb cross section excluding particle production, whereas the p-nucleus peak is 70 % or 200 mb of the 285 mb cross section. This comparison ignores the Pauli blocking of low momentum transfers to ^{12}C projectile

nucleons. We must remove the same low momentum transfers from the (p,p) cross section for a valid comparison. To achieve the same 29 % ratio as the ($^{12}\text{C}, ^{11}\text{B}+p$) cross section we use only the (p,p) cross section with $|t| < 0.022 \text{ GeV}^2$. This reduces the (p,p) peak to 30.6 mb of the remaining 106 mb cross section, and is equivalent to requiring that the scattered proton have a kinetic energy of at least 11.6 MeV in the projectile frame. This value was expected to equal 15.96 MeV, the Q value of the ($^{12}\text{C}, ^{11}\text{B}+p$) reaction.

Finally we show the proton cross section for an H target(Figure 11b). Here, if the proton were independent, we would expect to see only an $e^{5.2t}$ component. Instead there is an additional small peak which can not be fit by e^{86t} . So, while diffractive scattering can explain the C target low momentum transfer peak another mechanism is needed for the H target.

Such a mechanism could be excitation and decay via proton emission of the ^{12}C projectile, as in the nuclear Weiszäcker-Williams model[6] of Feshbach and Zabek. In this model the strong force “fringing field” of the target generates a “phonon” that is absorbed by the projectile which subsequently decays by emitting a nucleon pair to preserve momentum and energy balance. In our case the ^{12}C projectile decays into a proton and a ^{11}B . In this prescription the momenta of the proton and the ^{11}B are expected to be anticorrelated in the projectile rest frame(Figure 12a). The data (Figure 12b) show no obvious trend. The largest energy γ known to be emitted from an excited ^{11}B is 26.5 MeV[22] and would not materially effect the

anticorrelation.

The momentum transferred to the projectile has to be small compared with the separation momenta of the decay fragments or the anticorrelation is not observable. In the nuclear Weiszäcker-Williams model, energy transfers under 20 MeV would show no anticorrelation in our experiment. Perhaps the ^{11}B cannot survive intact at these energy transfers, making the model inapplicable here. However the anticorrelation should be visible in the $(^{12}\text{C}, p+p+^{10}\text{Be})$ reaction and it is not seen[23].

It should be noted that other forms of excitation and decay have not been ruled out, if they are associated with momentum transfers larger than that of the nuclear Weiszäcker-Williams model. Presumably, the 0.81 ± 0.45 mb peak in the H target data is due to such an excitation and decay. If this scales as the sum of the radii[3], then the 4.50 ± 0.67 mb peak in the C target is $27 \pm 16\%$ excitation and decay and $73 \pm 16\%$ diffractive scattering. This would make the Pauli blocking kinetic energy 14.4 MeV, considerably closer to the 15.96 MeV Q value it is expected to equal.

4 Conclusion

We find that the direct step of a peripheral relativistic heavy ion collision involves at least four mechanisms: (1) quasi-elastic nucleon-nucleon scattering, (2) inelastic nucleon-nucleon scattering with π production, (3) diffractive scattering, and (4) excitation and decay. The cross sections for the $(^{12}\text{C}, ^{11}\text{B}+p)$ reaction are 19.7 ± 3.4 mb for the H target and 39.7 ± 4.5 mb for the C target.

The free nucleon-nucleon prediction of the cascade model for quasi-elastic scattering between projectile and target nucleons is significantly different from the data. Although the model reproduces the shape of the data spectra we must multiply its cross section by 0.34 to obtain agreement. This suppression of the quasi-elastic component shows clearly that the cascade model is not a valid microscopic description of the interaction process. Also, a Fermi momentum of 190 MeV is needed. This reproduces the longitudinal momentum distribution of the proton spectra. However the transverse momentum distribution of the ^{11}B implies a Fermi momentum of 160 MeV. This discrepancy indicates that the usual assumption of the nucleus being a free Fermi gas of nucleons is inappropriate in this reaction. It has been suggested[16] that this discrepancy is due to the peripheral nature of the reaction, but no quantitative predictions have been made. The cross sections for the quasi-elastic component are 8.8 ± 2.5 mb for the $\text{H}(^{12}\text{C}, ^{11}\text{B}+p)\text{X}$ reaction and 11.1 ± 2.4 mb for the $\text{C}(^{12}\text{C}, ^{11}\text{B}+p)\text{X}$ reaction.

The free nucleon-nucleon prediction of the cascade model for the π production process does not reproduce the shape of spectra. However the cross section predicted for this inelastic process is much closer than the factor of three in the quasi-elastic fit. This inelastic component of the cascade model had to be multiplied by 0.70 for the H target data and by 0.95 for the C target data. The difference in shape between model and data results in residual data cross section at high rapidity loss indicating that other more highly inelastic processes must contribute to the inelastic region. The cross sections for this inelastic component are 10.1 ± 2.2 mb for the

H($^{12}\text{C},^{11}\text{B}+\text{p}$)X reaction, and 24.1 ± 3.7 mb for the C($^{12}\text{C},^{11}\text{B}+\text{p}$)X reaction.

Diffraction scattering, and excitation and decay are not independently resolvable for the C target since both produce a peak at low momentum and energy transfer. Excitation and decay is 0.81 ± 0.45 mb of 19.7 ± 3.4 mb in the H($^{12}\text{C},^{11}\text{B}+\text{p}$)X reaction. Assuming the process scales as the sum of the projectile and target radii, it is 1.21 ± 0.68 mb of the C($^{12}\text{C},^{11}\text{B}+\text{p}$)X reaction. This leaves 3.29 ± 0.96 mb of the reaction due to a proton in the ^{12}C projectile scattering diffractively from the C target.

5 Acknowledgments

We thank J. F. Gunion and T. F. Hoang for their insights on diffractive scattering. We also thank J. Alonso and the Bevatron Operations staff for the beam and support services, F. Bieser and I. Flores for the design and fabrication of the detector electronics, and E. Beleal, M. Bronson, and C. McParland for the data handling software. Finally, one of us (M.W.) thanks F. P. Brady and J. L. Romero for their guidance and support.

This work was supported in part by the Director, Office of Energy Research, Division of Nuclear Physics of the Office of High Energy and Nuclear Physics of the U. S. Department of Energy under Contracts DE-AC03-76SF00098 and DE-AS05-76ER04699, in part by NSF grant PHY81-21003, and in part by NASA grant NGR-05-003-513.

References

- [1] S. Nagamiya and M. Gyulassy, *Advances in Nuclear Physics* **13**, 201 (1984).
- [2] J. Papp, *Thesis, LBL Report LBL-3633* (1975).
H. Heckman and P. J. Lindstrom, *Physical Review Letters* **37**, 56 (1976).
L. Anderson, *Thesis, LBL Report LBL-6767* (1977).
M. Gazzaly et al., *Physics Letters* **79B**, 325 (1978).
S. Nagamiya et al., *Physical Review Letters* **45**, 602 (1980).
R. Stock et al., *Physical Review Letters* **44**, 1243 (1980).
I. Tanihata et al., *Physics Letters* **97B**, 363 (1980).
I. Tanihata et al., *Physics Letters* **100B**, 121 (1981).
Z. Zarbakhsh et al., *Physical Review Letters* **46**, 1268 (1981).
L. Anderson et al., *LBL Report LBL-14328* (1982).
- [3] P. J. Lindstrom et al., *LBL Report LBL-3650* (1975).
D. L. Olson et al., *Physical Review C* **28**, 1602 (1983).
- [4] D. Greiner et al., *Physical Review Letters* **35**, 152 (1974).
- [5] J. Hüfner, K. Schäfer and B. Schürmann, *Physical Review C* **12**, 1888 (1975).
- [6] H. Feshbach and M. Zabek, *Annals of Physics* **107**, 110 (1977).
H. Feshbach, *Progress in Particle and Nuclear Physics* **4**, 451 (1980).
- [7] J. Cugnon, *Physical Review C* **22**, 1885 (1980).
- [8] J. Engelage et al., *Physics Letters B* **173**, 34 (1986).
- [9] G. Chernov et al., *Nuclear Physics A* **280**, 478 (1977).
H. Heckman et al., *Physical Review C* **17**, 1651 (1978).
H. Heckman et al., *Physical Review C* **17**, 1735 (1978).
B. Jacobsson, *Physica Scripta* **17**, 491 (1978).
- [10] A. Sandoval et al., *Nuclear Physics A* **400** 365 (1983).
- [11] H. Crawford, *Lecture Notes in Physics* **178**, 92 (1983).
D. Greiner, *Nuclear Physics A* **400**, 325c (1983).
- [12] J. W. Harris, *personal communication*.
- [13] Particle Data Group, *UCRL Report UCRL-20000 NN* (1970).
- [14] P. J. Lindstrom et al., *14th International Cosmic Ray Conference* **7**, 2315 (1975).
- [15] E. J. Moniz et al., *Physical Review Letters* **26**, 445 (1971).

- [16] W. A. Friedman, *Physical Review C* **27**, 569 (1983).
- [17] J. F. Friedes et al., *Nuclear Physics A* **104**, 294 (1967). Original measurement.
W. Czyż et al., *Nuclear Physics B* **19**, 125 (1970). Data plotted in more convenient form.
- [18] K. Goulianos, *Physics Reports* **101**, 169 (1983).
- [19] W. Czyż, *Advances in Nuclear Physics* **4**, 61 (1971).
- [20] M. L. Good and W. D. Walker, *Physical Review* **120**, 1857 (1960).
- [21] J. Hüfner and M. C. Nemes, *Physical Review C* **23**, 2538 (1981).
B. Hiller and J. Hüfner, *Nuclear Physics A* **382** 542 (1982).
- [22] F. Ajzenberg-Selove and C. L. Busch, *Nuclear Physics A* **336**, 1 (1980).
- [23] H. J. Crawford, *private communication*.

Table Captions

Table I: Monte Carlo cascade model[7] cross section predictions for $^{11}\text{B}+x$ and $^{11}\text{B}+p$ production from H and C targets. From isospin considerations, for the H target, 1/4 of the proton-proton collisions resulting in Δ 's in the target also produce a proton in the projectile while 11/12 of the projectile Δ 's decay into a proton. For the C target 3/8 of the proton-nucleon collisions resulting in a target Δ leave a proton in the projectile while 17/24 of the projectile Δ 's decay into a proton. Also quasi-elastic charge exchange is $2.86 \pm 0.65\%$ [13] of quasi-elastic scattering from the C target. The cross sections have been normalized to total fragmentation cross sections of 250 ± 10 mb for a H target and 810 ± 20 mb for a C target[14].

Table II: Monte Carlo cascade model[7] cross section predictions for $^{11}\text{B}+p$ production in the proton aperture from H and C targets. These are compared to the data with the low momentum and energy transfer peak removed.

Table III: Aperture corrected cross section for $^{11}\text{B}+x$ and $^{11}\text{B}+p$ production from H and C targets. The peak cross section is measured. The quasi-elastic and inelastic cross sections are cascade model values scaled to fit the data inside the proton aperture.

Figure Captions

Figure 1: Detector Placement. Beam scintillators $TOF1$, TOT , HS , E , and DS defined the trigger with logic $(TOF1 \bullet TOT \bullet E \bullet \overline{HS} \bullet \overline{DS})$. Drift Chambers $DC4$, and $DC3$ determined the incoming ^{12}C trajectory and drift chambers $DC1$ and $DC2$ determined the charged projectile fragments' trajectories. The TOF wall, an array of 10 cm wide scintillators, determined the charge and time of flight for all projectile fragments.

Figure 2: Experimental aperture for protons shown as a function of rapidity and perpendicular momentum (a) parallel and (b) perpendicular to the dipole field. Drift chamber $DC2$ and the momentum reconstruction code were the limits to the acceptance. The crosses represent beam velocity protons. All ^{11}B were in the aperture.

Figure 3: Excitation energy for the $p, ^{11}\text{B}$ pair from (a) a H target and (b) a C target. Excitation energy is determined by finding the invariant mass of the projectile fragments and subtracting the ^{12}C rest mass.

Figure 4: Rapidity versus transverse momentum for protons from (a) a H target and (b) a C target. Contours units are $10^{-2}\text{mb}\cdot\text{rapidity}^{-1}\cdot(\text{MeV}/c)^{-1}$. The line shows the location of nucleon-nucleon quasi-elastic scattering.

Figure 5: Rapidity versus transverse momentum for ^{11}B inclusive from (a) a H target and (b) a C target: The beam rapidity was 1.84. Contours units are $10^{-1}\text{mb}\cdot\text{rapidity}^{-1}\cdot(\text{MeV}/c)^{-1}$.

Figure 6: Rapidity versus transverse momentum for ^{11}B inclusive from the Monte Carlo cascade model for a H target. The data (Figure 4) has a high transverse momentum tail this model lacks. Contours units are $10^{-1}\text{mb}\cdot\text{rapidity}^{-1}\cdot(\text{MeV}/c)^{-1}$.

Figure 7: Rapidity versus transverse momentum for protons from the Monte Carlo cascade model for (a) quasi-elastic scattering and (b) inelastic scattering with π production from the H target. Also shown are plots summing both processes from (c) H and (d) C targets. These should be compared with the data (Figure 4). Contours units are $10^{-2}\text{mb}\cdot\text{rapidity}^{-1}\cdot(\text{MeV}/c)^{-1}$.

Figure 8: Monte Carlo cascade model normalized to the data as a function of $-t$ for (a) H and (b) C targets. Here t is a modified Mandelstam $t = (\mathbf{p}_1 - \mathbf{p}_3)^2$, where $\mathbf{p}_1 = \mathbf{p}_{\text{beam}}/12$ before the reaction and $\mathbf{p}_3 = \mathbf{p}_{\text{proton}}$ after the reaction. The reduced mass of a nucleon within a ^{12}C nucleus is accounted for by using $\mathbf{p}_{\text{beam}}/12$. All \mathbf{p} are four-vectors. The lines are natural spline fits to the normalized Monte Carlo cascade model.

Figure 9: Rapidity versus transverse momentum for protons from the data with the Monte Carlo cascade model subtracted for (a) H and (b) C targets. The main features are: residual inelastic cross section in the low rapidity region and the low momentum transfer peaks. Contours units are $10^{-2}\text{mb}\cdot\text{rapidity}^{-1}\cdot(\text{MeV}/c)^{-1}$.

Figure 10: $C(p,p)X$ cross section versus Mandelstam $-t$ [17]. The line, $\sigma(t) = 17.22e^{86t} + 0.44e^{5.2t}$, is a fit to the data points.

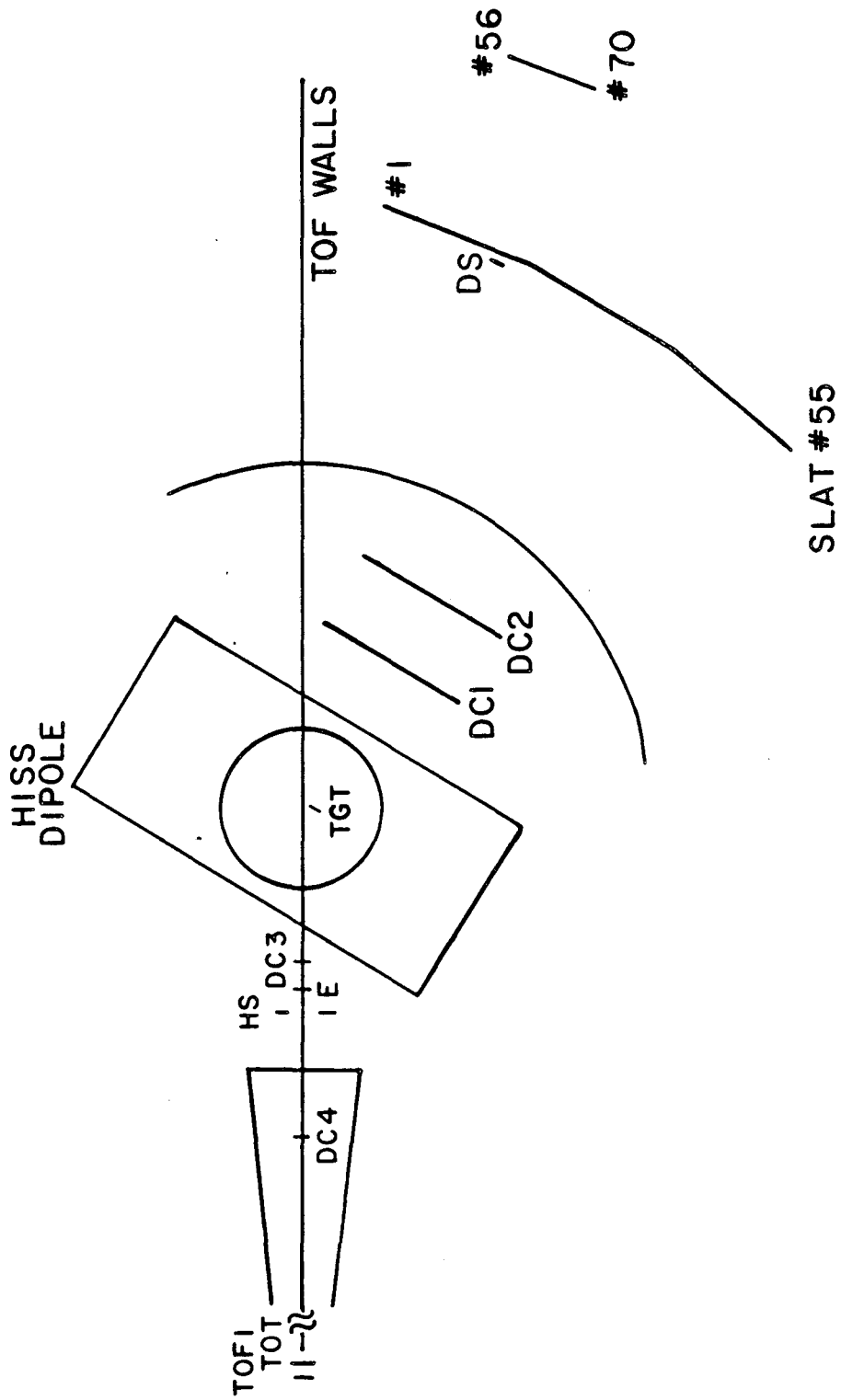
Figure 11: Data cross section versus modified $-t$ for (a) C and (b) H targets. The solid lines are natural spline fits to the normalized Monte Carlo cascade model. The dashed line shows the effect of adding an e^{86t} component to the Monte Carlo cascade model results.

Figure 12: Perpendicular momenta, ^{11}B versus proton, parallel to the dipole field to maximize resolution. (a) Nuclear Weiszäcker-Williams model. (b) Carbon target. Contours units are $10^{-5}\text{mb}\cdot(\text{MeV}/c)^{-2}$.

Monte Carlo cascade model process cross sections	H Target (mb)		¹² C Target (mb)	
	¹¹ B+x	¹¹ B+p	¹¹ B+x	¹¹ B+p
Nucleon-nucleon elastic scattering	25.6±1.1	25.6±1.1	33.99±0.93	33.02±0.93
Δ production in the projectile	12.30±0.52	11.28±0.48	23.43±0.67	16.59±0.47
Δ production in the target	12.30±0.52	3.08±0.13	23.43±0.67	8.79±0.25
Model total	50.2±2.0	39.9±1.6	80.8±2.1	58.4±1.5
Measured total	30.9±3.4	—	53.8±2.7	—

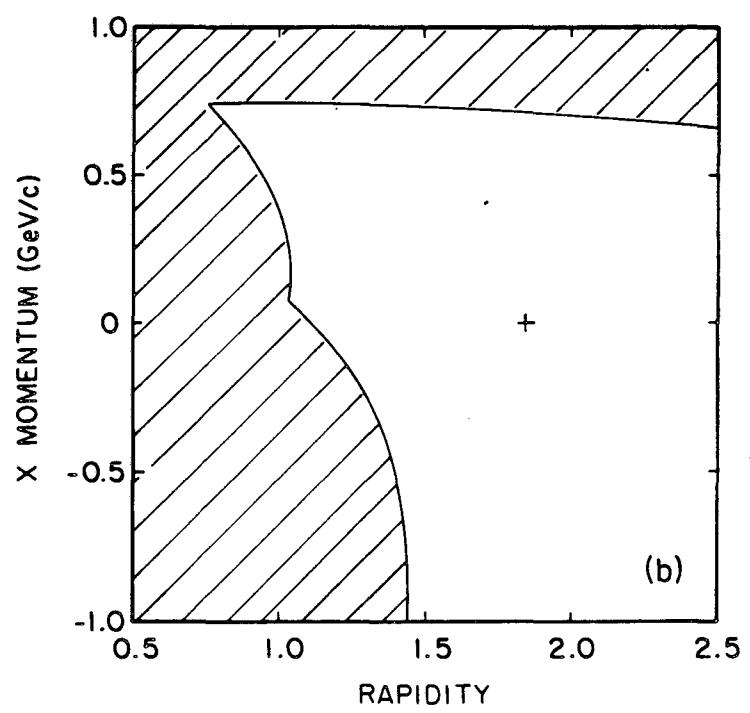
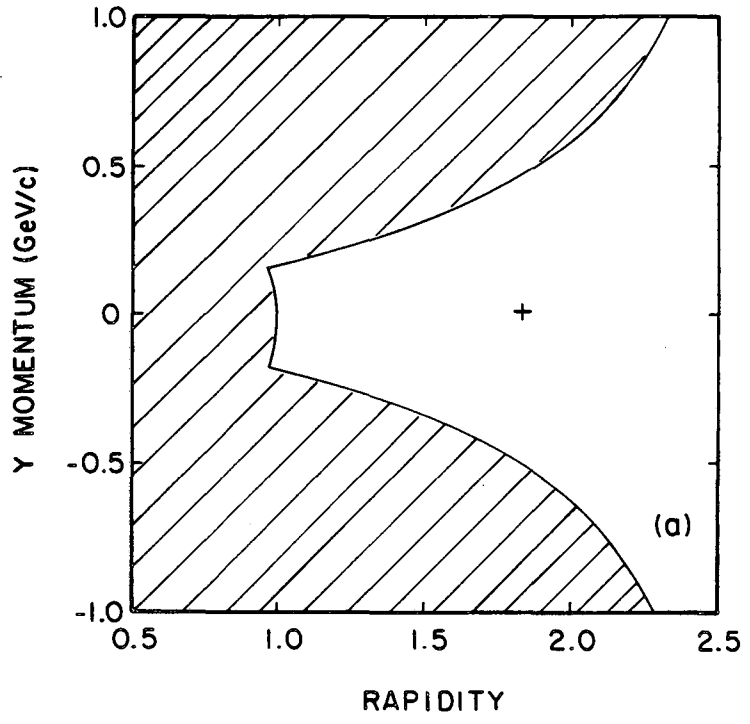
Monte Carlo cascade model process cross sections in aperture	H Target (mb)		¹² C Target (mb)	
	Unscaled	Scaled	Unscaled	Scaled
Nucleon-nucleon elastic scattering	21.16±0.88	7.3±2.1	26.02±0.75	8.7±1.9
Δ production in the projectile	8.98±0.39	6.3±1.4	7.76±0.25	7.3±1.4
Δ production in the target	2.53±0.11	1.77±0.40	4.70±0.15	4.45±0.84
Model total	32.7±1.3	15.3±2.7	38.5±1.0	20.5±2.9
Measured total – peak	—	15.8±3.4	—	21.4±2.0

Aperture corrected process cross sections	H Target (mb)		¹² C Target (mb)	
	¹¹ B+x	¹¹ B+p	¹¹ B+x	¹¹ B+p
Low momentum transfer peak	0.81±0.45	0.81±0.45	4.50±0.67	4.50±0.67
Nucleon-nucleon elastic scattering	8.8±2.5	8.8±2.5	11.4±2.5	11.1±2.4
Δ production in the projectile	8.6±1.9	7.9±1.8	22.2±3.4	15.7±2.4
Δ production in the target	8.6±1.9	2.16±0.48	22.2±3.4	8.3±1.3
Aperture corrected total	26.7±4.6	19.7±3.4	60.3±7.3	39.7±4.5
Measured total	30.9±3.4	—	53.8±2.7	—



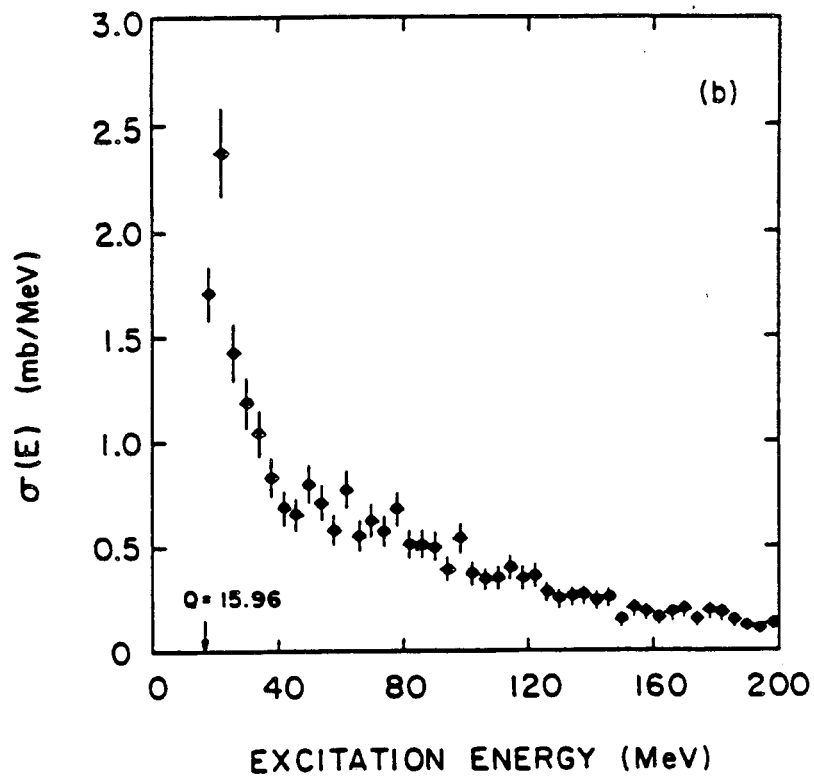
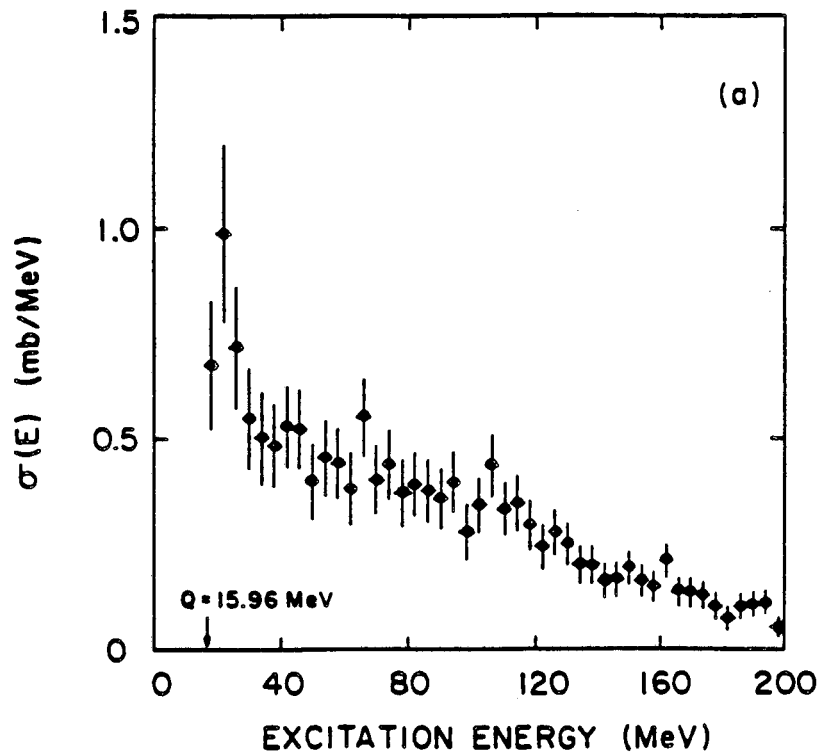
XBL 8311-4605

Figure 1



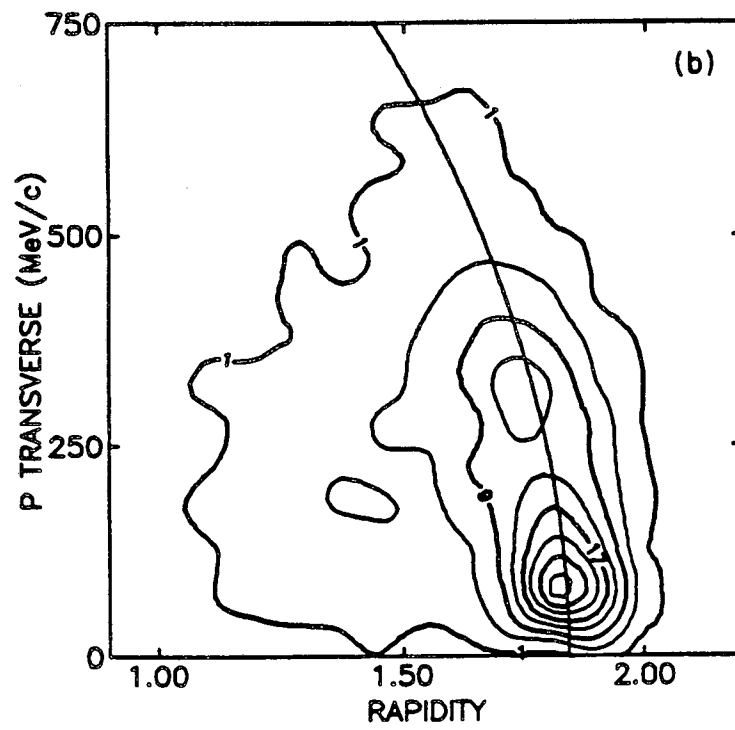
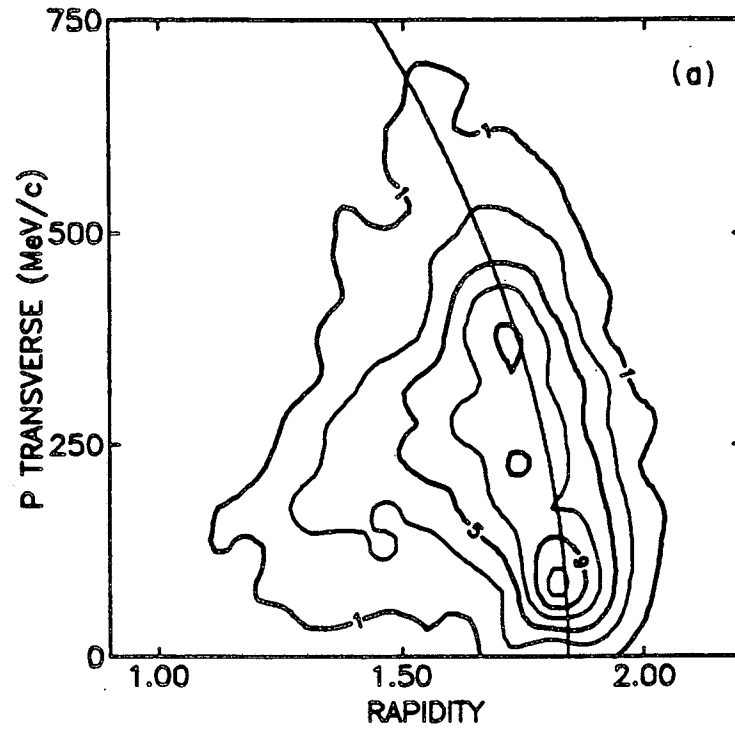
XBL 8610-3767

Figure 2



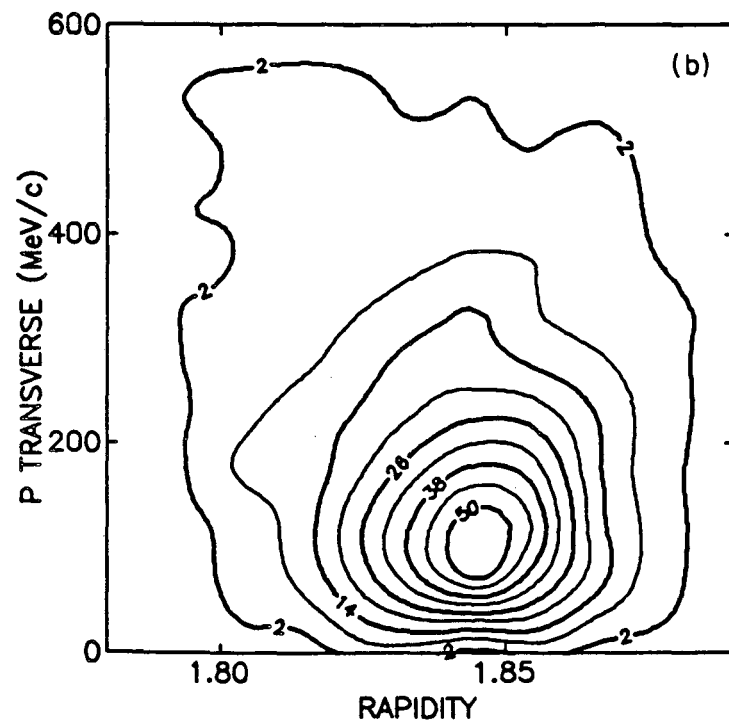
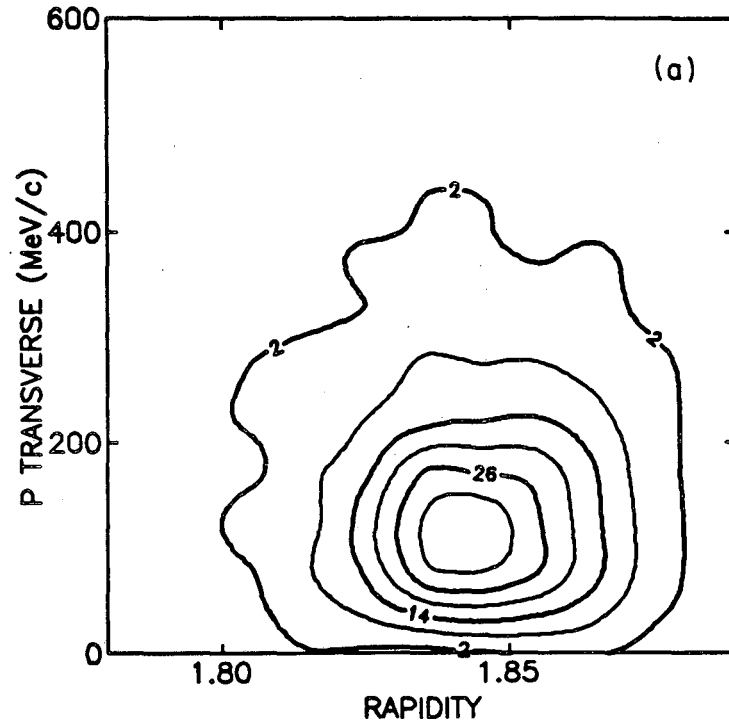
XBL 8611-4718

Figure 3



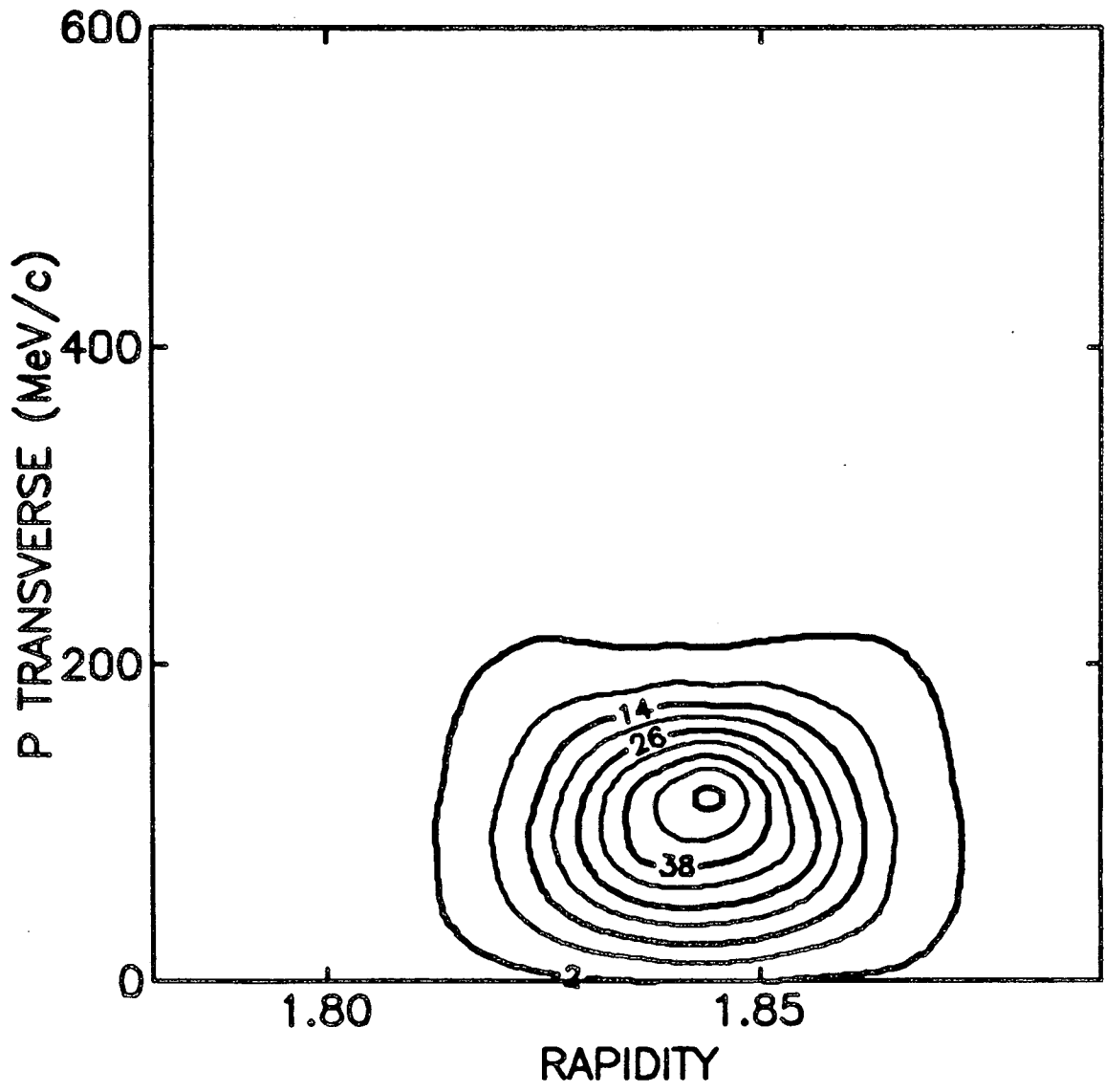
XBL 8611-4719

Figure 4



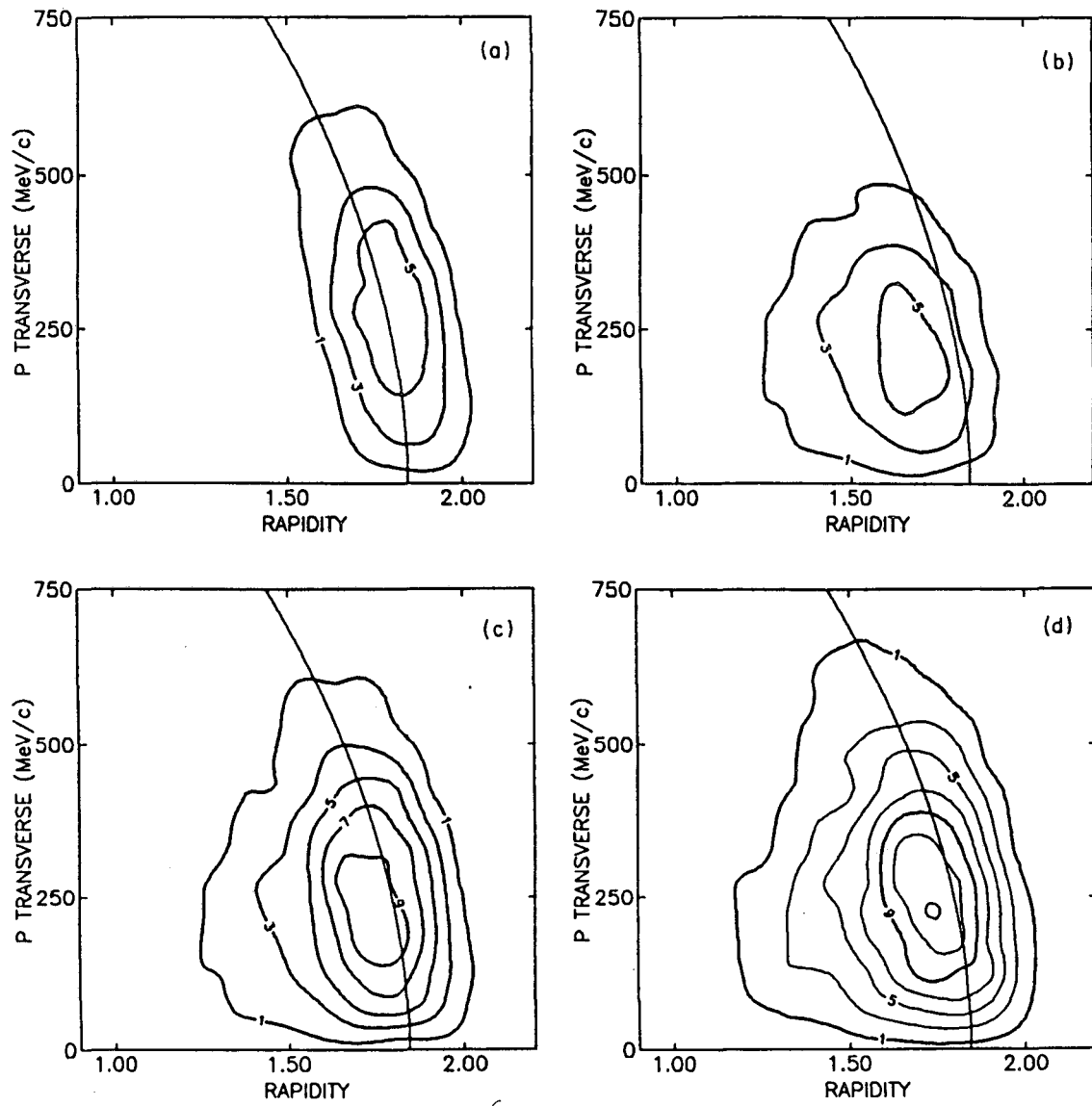
XBL 8611-4720

Figure 5



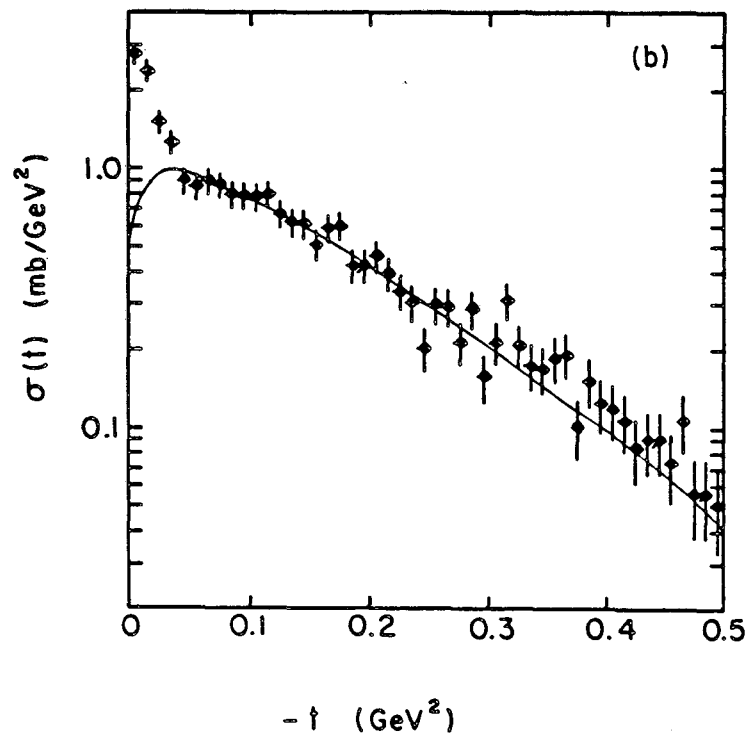
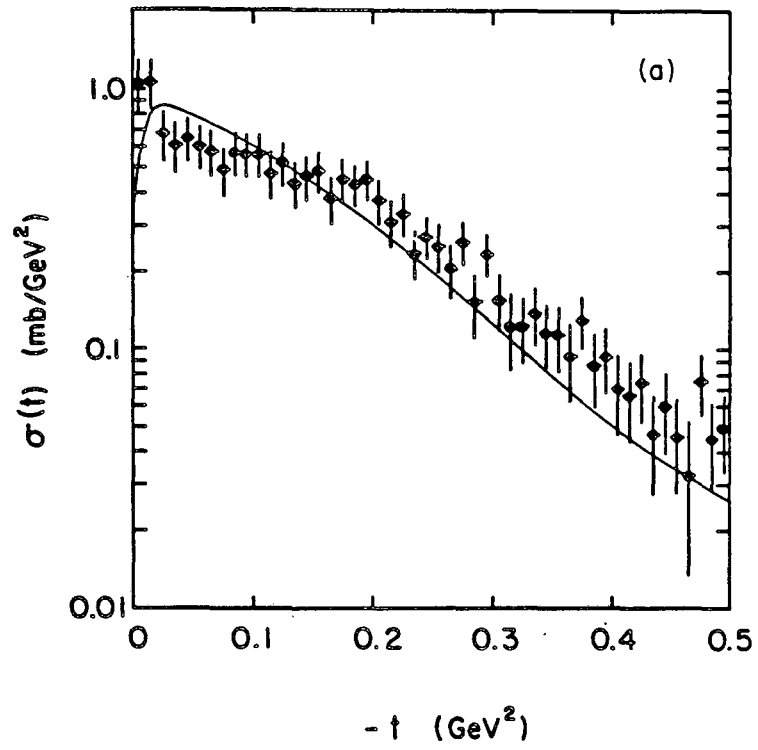
XBL 8611-4722

Figure 6



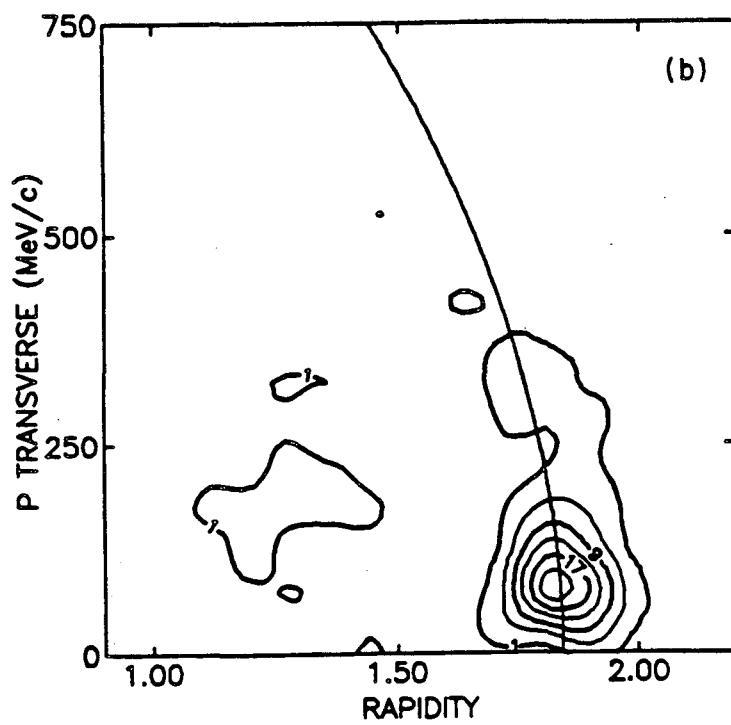
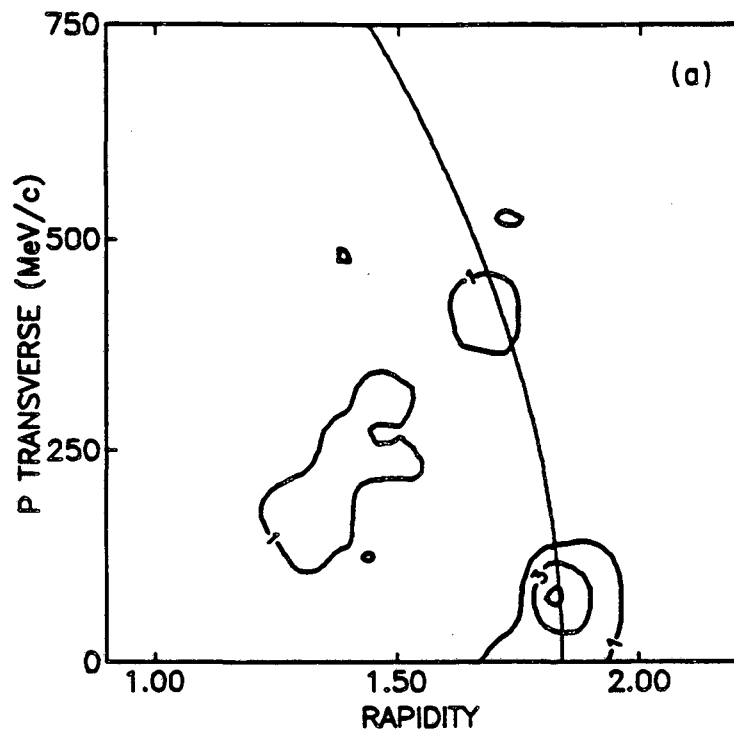
XBL 8611-4723

Figure 7



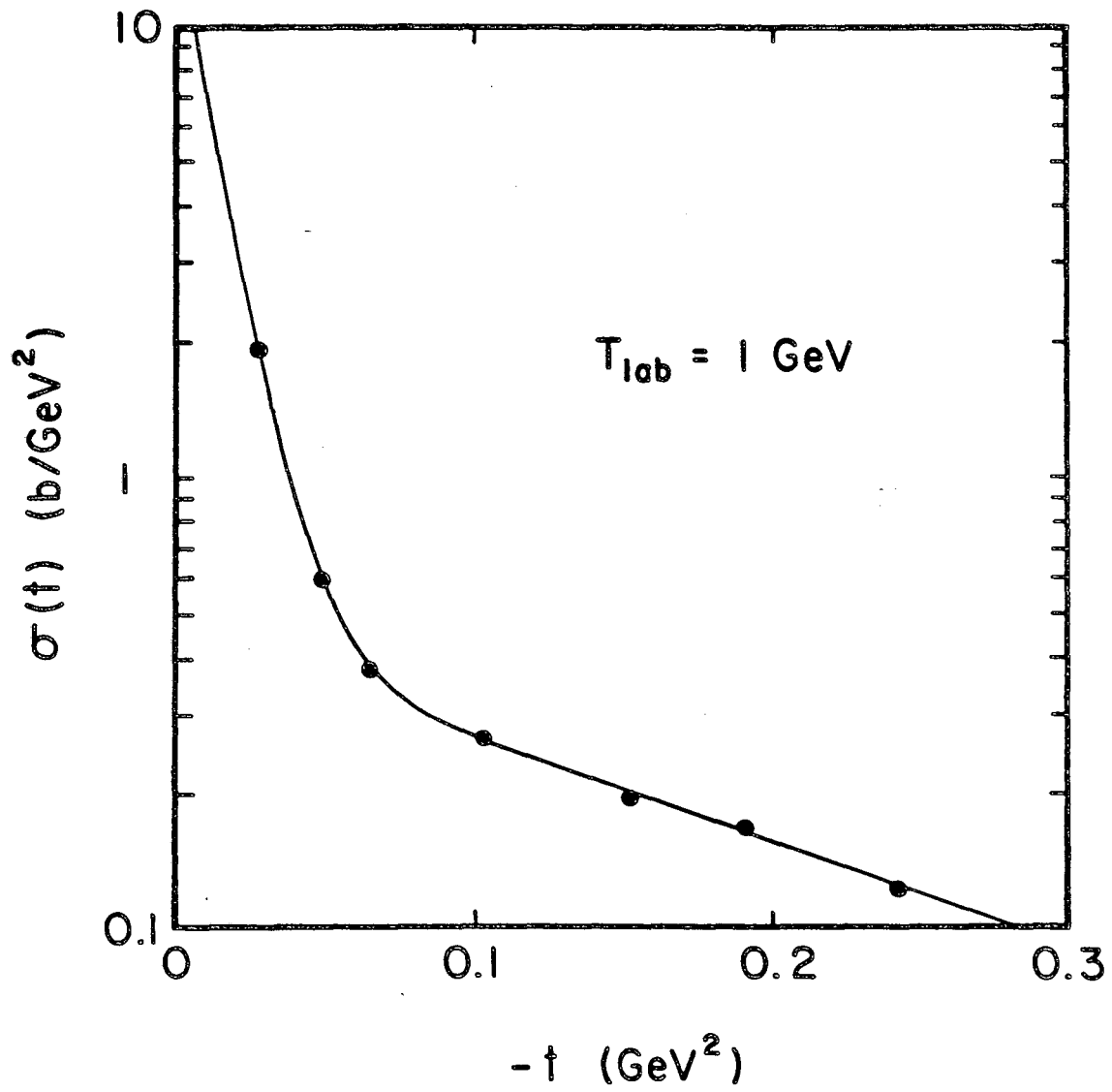
XBL 8612-4814

Figure 8



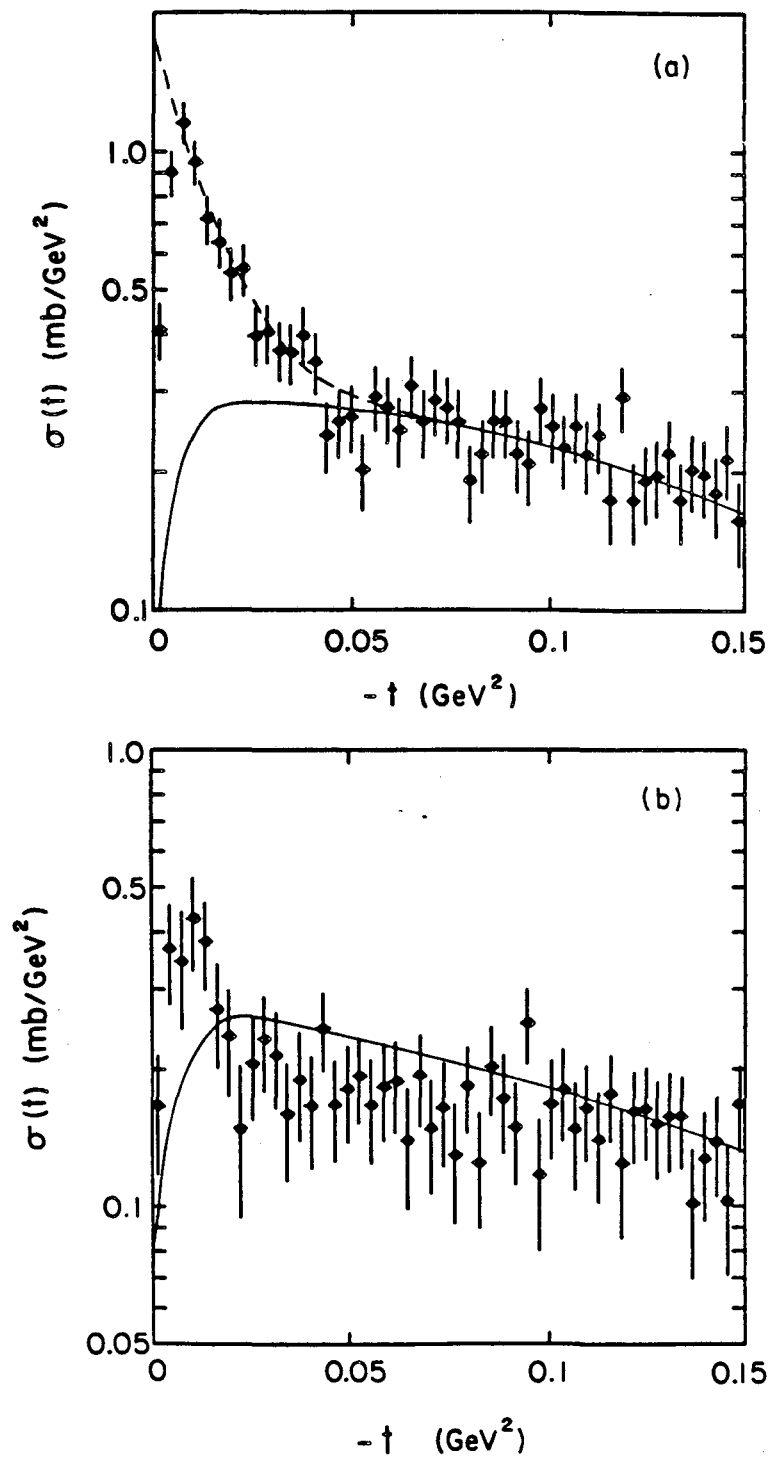
XBL 8611-4721

Figure 9



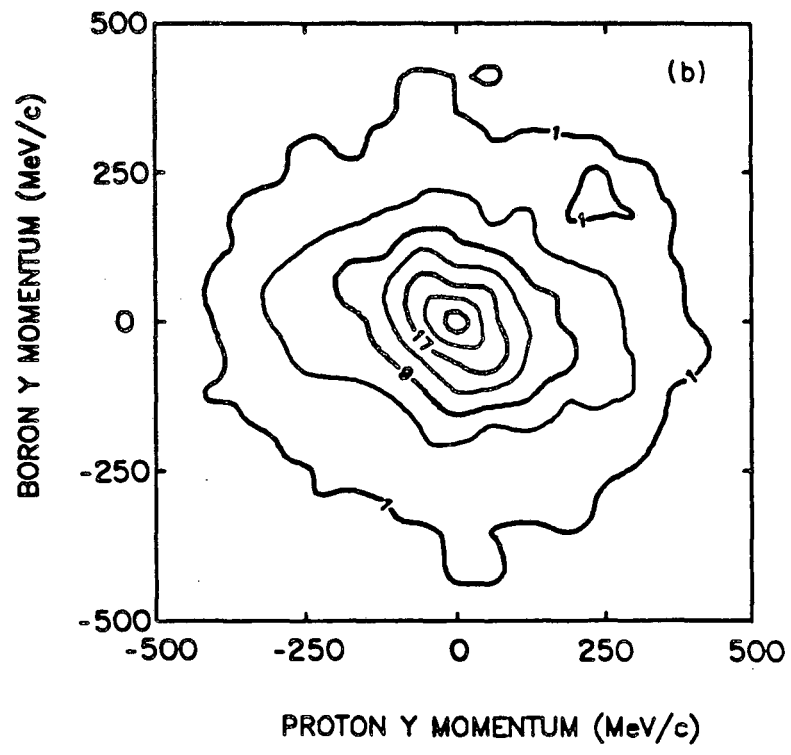
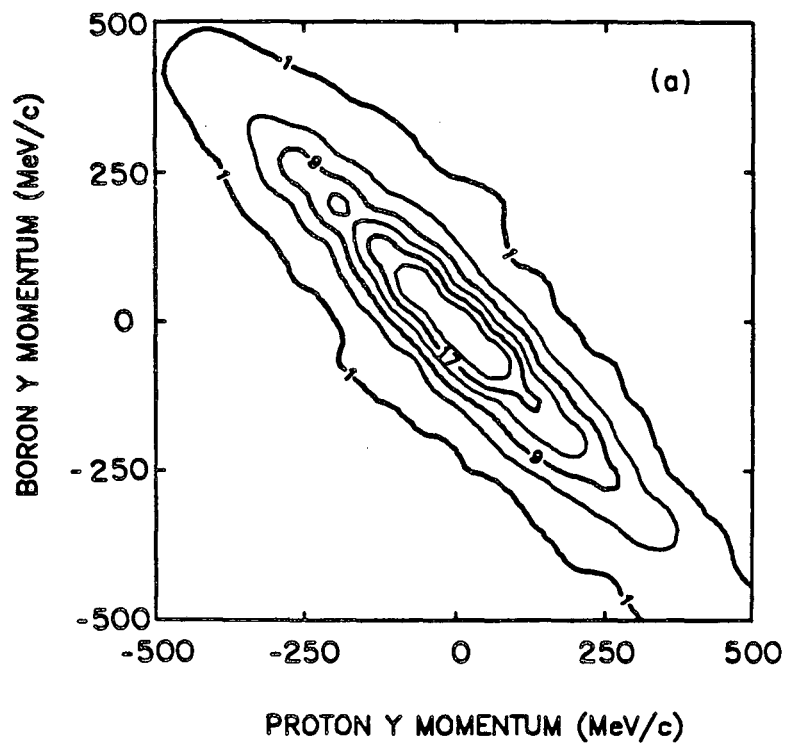
XBL 8612-4813

Figure 10



XBL 8612-4815

Figure 11



XBL 8612-4812

Figure 12

This report was done with support from the Department of Energy. Any conclusions or opinions expressed in this report represent solely those of the author(s) and not necessarily those of The Regents of the University of California, the Lawrence Berkeley Laboratory or the Department of Energy.

Reference to a company or product name does not imply approval or recommendation of the product by the University of California or the U.S. Department of Energy to the exclusion of others that may be suitable.

*LAWRENCE BERKELEY LABORATORY
TECHNICAL INFORMATION DEPARTMENT
UNIVERSITY OF CALIFORNIA
BERKELEY, CALIFORNIA 94720*